MARS SCIENCE LABORATORY ORBIT DETERMINATION

Gerhard L. Kruizinga[1], Eric D. Gustafson[2], Paul F. Thompson[3], David C. Jefferson[4], Tomas J. Martin-Mur[5], Neil A. Mottinger[6], Frederic J. Pelletier[7], and Mark S. Ryne[8]

[1-8] *Jet Propulsion Laboratory, California Institute of Technology, 4800 Oak Grove Drive, Pasadena, California 91109, +1-818-354-7060, {Gerhard.L.Kruizinga, edg, Paul.F.Thompson, David.C.Jefferson, tmur, Neil.A.Mottinger, Fred.Pelletier, Mark.S.Ryne}@jpl.nasa.gov*

Abstract: *This paper describes the orbit determination process, results and filter strategies used by the Mars Science Laboratory Navigation Team during cruise from Earth to Mars. The new atmospheric entry guidance system resulted in an orbit determination paradigm shift during final approach when compared to previous Mars lander missions. The evolving orbit determination filter strategies during cruise are presented. Furthermore, results of calibration activities of dynamical models are presented. The atmospheric entry interface trajectory knowledge was significantly better than the original requirements, which enabled the very precise landing in Gale Crater.*

Keywords: *Mars Science Laboratory, Curiosity, Mars, Navigation, Orbit Determination*

1. Introduction

On August 6, 2012, the Mars Science Laboratory (MSL) and the Curiosity rover successful performed a precision landing in Gale Crater on Mars. A crucial part of the success was orbit determination (OD) during the cruise from Earth to Mars. The OD process involves determining the spacecraft state, predicting the future trajectory and characterizing the uncertainty associated with the predicted trajectory. This paper describes the orbit determination process, results, and unique challenges during the final approach phase.

1.1. MSL Mission Overview

On November 26, 2011, the Mars Science Laboratory was launched from Cape Canaveral on a Type I trajectory. The cruise phased ended successfully with a precise landing on Mars in Gale Crater on August 6, 2012. Orbit determination played a pivotal role during the launch, cruise, approach and entry phase, which included trajectory reconstruction and prediction including trajectory uncertainty propagation. MSL was launched in a biased trajectory missing Mars by a safe distance to meet planetary protection requirements for avoiding impact of the MSL upper stage [1]. A summary of major navigation-related events during cruise is given in Tab. 1.

Table 1: MSL major navigation cruise events

Mission Event	Mission Event Date	Relative Mission Time	Comment
Launch	26-Nov-11	L+0 days	Launch from Cape Canaveral 15:02 UTC
Lateral Calibration	22-Dec-11	L+25 days	
TCM-1	11-Jan-12	L+45 days	
ACS/NAV Calibration	25-Jan-12	L+59 days	
TCM-2	26-Mar-12	L+120 days	
TCM-3	26-Jun-12	E-40 days	
TCM-4	29-Jul-12	E-8.0 days	
EPU-1	30-Jul-12	E-6.5 days	Event refers to tracking data cut off
TCM-5	04-Aug-12	E-2.0 days	Waived
EPU-2	04-Aug-12	E-33 hours	Waived
EPU-3	05-Aug-12	E-15 hours	Waived
TCM-6	05-Aug-12	E-9 hours	Waived (contingency maneuver)
EPU-4	05-Aug-12	E-6 hours	Waived
Entry	06-Aug-12	E-0 hours	Entry at 05:10:45 UTC

The MSL spacecraft was the first mission to use entry guidance at Mars to meet the precise landing requirements for Gale Crater. In previous Mars missions Phoenix and the Mars Exploration Rovers (MER), the navigation objective was to control the entry state such that in a mean sense, the desired landing location would be achieved assuming ballistic entry without any control, resulting in large landing uncertainty ellipses. For MSL, the guidance system used active control to land at a desired location by processing Inertial Measurement Unit (IMU) data, but the guidance system needed to be initialized with the entry state. Therefore, the emphasis of the MSL OD team at the end of the approach

phase was focused on trajectory knowledge and not controlling the landing location on the surface. Before launch, four Entry Parameter Updates (EPU), which include the entry state, were planned. The first of these updates, EPU-1, based on tracking data up to Entry-6.5 days, was uploaded on July 30, 2012. All other EPU opportunities were canceled due to stability of the OD solution for the remainder of the approach phase up to atmospheric entry.

The Trajectory Correction Maneuvers (TCM) 1, 2 and 3 were initially designed to be optimized together to remove the trajectory bias. However, due to a very good injection, TCM-2 was designed to directly target the atmospheric entry interface of the Gale Crater landing site. In early cruise, a calibration of the Attitude Control System (ACS) thrusters was performed to assess the amount of ΔV imparted on the spacecraft during a spacecraft turn due to thruster imbalance. In mid and late cruise, an extensive campaign was conducted by the OD team to refine models for non-conservative forces and optimization of the filter strategy. In the approach phase, only one course correction was necessary (TCM-4 at Entry-8 days) because of the early entry interface targeting of TCM-2 and TCM-3. This resulted in a small TCM-4 ΔV and therefore small TCM-4 execution errors. Furthermore, this also resulted in the cancellation of TCM-5 at Entry-2 days and the contingency TCM-6 at Entry-9 hours. Figure 1 shows the OD progression in the B-plane at key points during the mission.

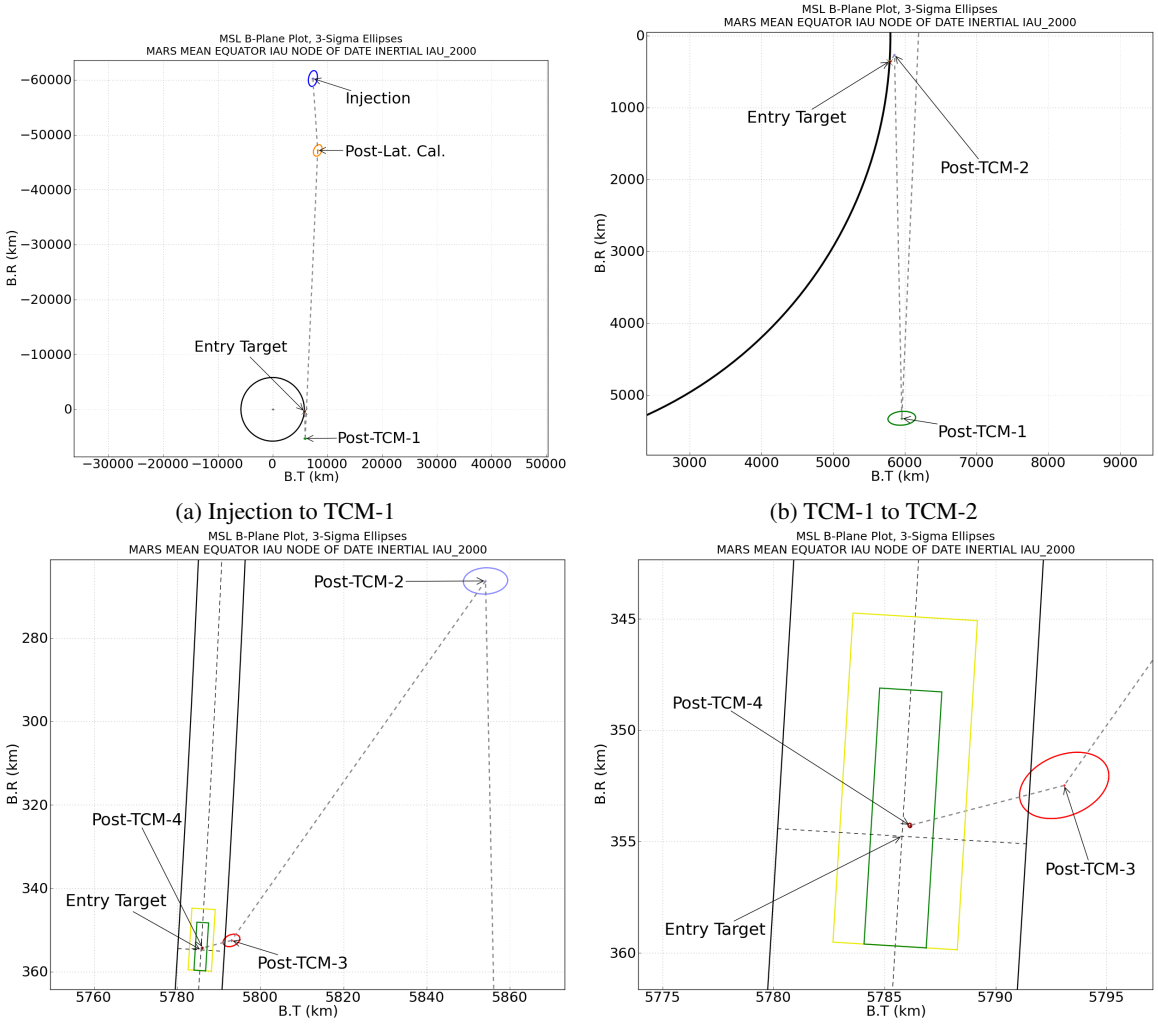

(a) Injection to TCM-1

(b) TCM-1 to TCM-2

(c) TCM-2 to TCM-3

(d) TCM-3 to Entry

Figure 1: Mission Overview B-plane

The 3-σ requirements for OD were to provide an entry state with an accuracy of 2.8 km in position, 2.0 m/sec in velocity and a flight path uncertainty of 0.2°. In Fig. 1 and all following figures, the 0.2° uncertainty flight path angle uncertainty corridor is shown in black. After launch, a set of TCM-5 decision criteria were defined with the Entry

Descent and Landing (EDL) team, which are visible in Figs. 1c and 1d. The green box TCM-5 decision criteria was defined by $\pm 0.05^\circ$ in flight path angle and in cross track 3 km to the south and 4 km to the north. If the OD solution fell within the green box, no TCM-5 maneuver would be executed. The yellow box TCM-5 decision criteria was defined by $\pm 0.1^\circ$ in flight path angle and in cross track 3 km to the south and 6 km to the north. If the OD solution were within the yellow box but outside the green box then a TCM-5 would only be executed if the spacecraft was healthy. Outside the yellow box a TCM-5 would be executed regardless of spacecraft health.

1.2. Spacecraft Description

The MSL spacecraft in cruise configuration is shown in Fig. 2. The spacecraft consist out of four components: cruise stage, aeroshell, descent stage and the rover, which are described in more detail in [2]. As the name suggests, the cruise stage housed the antennas and thrusters used during interplanetary cruise: a Low Gain Antenna (LGA) for early cruise operations, a Medium Gain Antenna (MGA) for farther distances, and two diametrically opposed thruster cluster assemblies. Each thruster cluster assembly contains four thrusters. For attitude determination, the cruise stage has Sun sensors and one star scanner. Also in the cruise stage are two propellant tanks containing about 72 kg of hydrazine. The total mass of the spacecraft was modeled to be 3838.7 kg at launch and reduced with the reported propellant mass consumption for each propulsive event during cruise. The total modeled spacecraft mass at entry, before the start of the EDL sequence, was 3811.1 kg based on an overall propellant mass consumption of 27.6 kg.

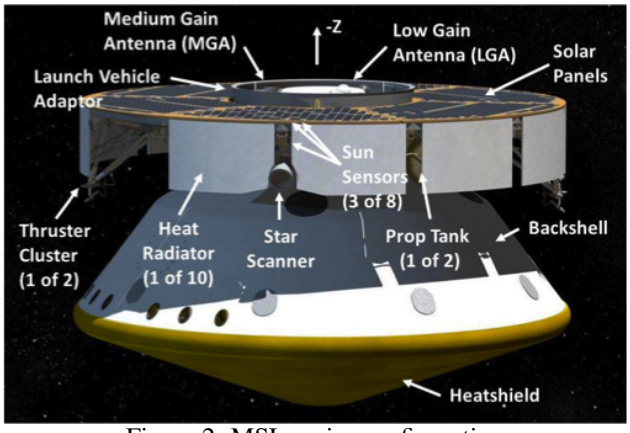

Figure 2: MSL cruise configuration

The MSL spacecraft was spin-stabilized at 2 RPM, introducing a periodic signature in the tracking data and a Doppler bias related to the magnitude of the spin rate. The MSL OD team developed a new tool that could estimate the spacecraft spin state, remove the periodic signature from all radiometric Deep Space Network (DSN) tracking data and correct the Doppler bias due to the spacecraft spin. Unlike previous spin-stabilized Mars missions, the tracking data were corrected for spin during launch, improving the accuracy of the early trajectory reconstruction. The spin signature removal tool also provided additional data to the ACS team to aid in spacecraft attitude reconstruction and spacecraft event timing for the remainder of the mission.

2. Dynamics and Measurement Modeling

This section describes the dynamic models that were used in the MSL OD process, namely gravity, ACS turn ΔVs, TCM ΔVs, and solar radiation pressure (SRP). The measurement model includes DSN stations coordinates and the quasar catalog. All modeling was performed with JPL's MONTE (Mission-analysis, Operations, and Navigation Toolkit Environment) software [3].

The MSL OD process used dedicated planetary ephemerides, which were focused on improving the Mars ephemerides with the latest observations. The Planetary ephemerides used were DE424 [4] which was delivered 2 months prior to MSL launch and DE425 [5] which was delivered 3 months before entry. The planetary ephemerides covariance used was from DE423 [6] for the complete mission. The gravitational parameter (GM) values and uncertainties were based on DE424 except for the Earth-Moon system and Mars, for which the values listed in the Mars Science Laboratory

Planetary Constants and Models Document [7] were used. The spherical harmonic expansions of the Earth, Moon, and Mars gravity fields were all truncated to degree and order 8, taken from models GGM02C [8], LP150q [9], and mgs95j [10], respectively.

The MSL OD team used a novel approach for modeling the SRP in interplanetary navigation. Most interplanetary missions model the SRP using a geometric model of the spacecraft and assign to each surface optical properties to compute the SRP force. In Fig. 3, the MSL spacecraft is depicted showing all the possible SRP forces and surfaces involved. Modeling each surface and SRP force becomes rather complex with a complicated spacecraft geometry. For MSL, the SRP is computed by expanding the net total SRP force into Fourier series as a function of the Solar colatitude because MSL is a spin-stabilized spacecraft rotating approximately about the Z-axis. The Fourier coefficients represent the effective surface areas. In the MSL SRP model, the sum of the Fourier coefficients are multiplied by an appropriate scale factor to account for the spacecraft mass, solar distance and solar flux. The SRP is calculated in the MSL Solar Frame, where the Z-axis is the spacecraft -Z axis, the Y axis is the perpendicular to the plane containing the Sun vector and the spacecraft -Z axis and X completes the right-handed MSL Solar frame. Thus, the SRP Z-axis Fourier coefficients represent the SRP force in approximately the rotation axis (Z-axis) direction and the SRP X-axis Fourier coefficients represent the SRP force perpendicular to the rotation axis in the plane formed by the Sun vector and the spacecraft Z-axis. Furthermore, the Y-axis represents the SRP force perpendicular to the plane formed by the Sun vector and the spacecraft Z-axis. In general, this force is expected to be small because of the spacecraft symmetry but thermal imbalance may cause a force in this direction, for example the Yarkovsky effect [11]. Prior to launch, a MSL geometric model was constructed with appropriate surface optical modeling and a MSL Fourier expansion SRP was estimated up to degree 2 for only the X and Z coefficients. The MSL SRP model fit to the geometric model was better than 0.03%. This MSL SRP fit was used as the *a priori* model during launch and early cruise in the OD process.

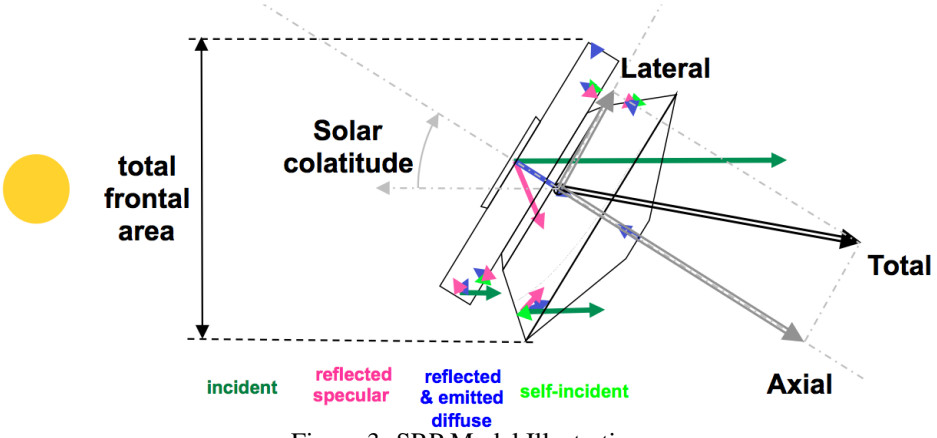

Figure 3: SRP Model Illustration

Initially during cruise, significant outgassing prevented the accurate estimation of the MSL SRP model parameters and additional stochastic accelerations were estimated. After outgassing subsided, it was realized that thermal radiation from the Radioisotope Thermoelectric Generator (RTG) did not average out in the spacecraft Z-axis. Since this radiation is independent of distance to the Sun and solar flux, the dynamics model was augmented with a constant stochastic Z-axis acceleration and estimated as part of the OD process during late cruise and approach.

During cruise, MSL executed spacecraft turns using the ACS thrusters to meet communication and thermal requirements. The ACS turns were modeled as small impulsive burns for the X, Y and Z axes of the MSL ACS Turn Frame. The MSL ACS Turn Frame is defined as an inertial frame that coincides with mean position of the spacecraft coordinate frame axes during a turn. The TCMs can be executed in several modes: axial only (thrusting along the rotation axis), lateral only (thrusting perpendicular to the rotation axis) and a combination of axial and lateral, called vector mode. Since MSL is a spinning spacecraft, the lateral maneuver may take a long time because only twice during each revolution the thruster can be activated for a short time. Therefore, the lateral maneuver is executed in segments to allow the spacecraft to dampen any unwanted attitude variations that occurred during a segment. For the OD process, each segment was modeled separately since a small amount of Doppler tracking data was available between segments. All TCM segments were modeled as finite burns where *a priori* maneuver design was converted into right ascension, declination, ΔV and

burn start time in the EME2000 inertial coordinate frame [12]. In the OD process, these parameters were then estimated with appropriate parameter constraints.

3. Radiometric Tracking Data

The navigation solutions for MSL were based entirely on the radiometric tracking data types of two-way coherent Doppler, two-way coherent ranging, and Delta-Differential One-way Ranging (ΔDOR). Each data type gives unique information about the spacecraft's trajectory: Doppler measurements give line-of-sight velocity, ranging gives line-of-sight distance, and ΔDOR gives plane-of-sky direction. See Martin-Mur [2] for more details and a data tracking schedule. The DSN stations coordinates for processing of the DSN Doppler and Range were taken from [13] and associated covariance. The ΔDOR processing used quasar locations provided by the DSN [14].

3.1. Spin Signature Removal

MSL was spin-stabilized during its cruise to Mars, just like the two MER spacecraft preceding it [15]. Spin-stabilization provides many advantages that simplify cruise operations, but it also makes processing the navigation radiometric data more complicated. The spin produces two main effects in the data: a periodic signature and a frequency bias. For MSL, the rotational motion of the spacecraft was modeled as a rigid body, then the data were corrected given the full antenna motion including nutation.

The OD team pre-processed the raw high-rate data in a process called "despinning." During despinning, the raw tracking data received from the rotating antenna was modified to be representative of the non-rotating center of mass of the spacecraft. Once that was accomplished, the Doppler data could be compressed without any loss of information.

Uncertainty of the spin rate was typically as low as micro-degrees per second. During the period shortly after MSL's launch, a small spin acceleration was detected, possibly due to outgassing. Even though the magnitude of this spin acceleration was about 4×10^{-9} deg/sec^2, it was clearly evident in the data.

Additionally, the despinning process had unplanned benefits. The spacecraft team used the despinning process to perform independent validation of the method used to obtain spacecraft clock correlation. By comparing the spin phase derived from the OD despinning to the spin phase from the ACS telemetry, an estimate could be obtained of the difference between the spacecraft clock and the DSN clocks.

The despin process also proved beneficial for attitude verification. For the purpose of preparing data for OD, despinning was done one DSN pass at a time. This 8-hour time span allows for an accurate estimate of the angle between the Earth and the spin axis, which is not sufficient to determine the full spin axis direction. However, by despinning a long duration of data (about a week), the geometry changed enough such that Doppler measurements provide enough observability to estimate the full attitude of the spin axis. The OD-based spin axis estimate agreed with the ACS telemetry extremely well, giving both teams confidence in their methods.

4. Orbit Determination Filter Strategy and Results

In this section, the OD filter strategy and OD results are presented from MSL launch to entry. The OD process strategy evolved with each phase of the cruise mission because of unique aspects of that phase or lessons learned in previous phases, which were carried forward. For this discussion, the cruise mission is divided up into the following phases: launch, early cruise, mid-cruise, late cruise and final approach. The timespan for each phase is defined in Tab. 2. For each phase, the filter strategy will be presented in table form along with a discussion of how the filter strategy changed and the reasoning for the changes

A key characteristic of any OD solution is the timespan of data included in the solution. The last time at which measurements are included in the data set is called the data cutoff (DCO). For each DCO, several OD solutions were computed by using various data start times. These different starting times define different "data arcs", summarized in Tab. 3. One of these arcs was chosen to be the officially delivered OD solution for each DCO. Any specific phase event result, for example TCMs or calibrations, will be discussed in subsections.

Table 2: Orbit determination phase definitions

Phase	Start Date	End Date	Comment
Launch	26-Nov-2011	26-Nov-2011	First tracking pass
Early Cruise	26-Nov-2011	11-Jan-2012	Launch to TCM-1
Mid-Cruise	11-Jan-2012	05-Mar-2012	Starts at TCM-1
Late Cruise	05-Mar-2012	29-Jul-2012	Ends at TCM-4
Final Approach	29-Jul-2012	06-Aug-2012	TCM-4 to Entry

Table 3: Orbit determination arc list

Arc Designation	Arc Start Time (UTC)	Comment
A	29-Nov-2011	Launch + 3.3 days
B	29-Nov-2011	Arc not used for OD deliveries
C	22-Dec-2011	Post lateral calibration
D	12-Jan-2012	Post TCM-1
E	28-Feb-2012	Post MGA antenna switch
F	10-Apr-2012	Post IMU calibration 2
G	26-Jun-2012	Post TCM-3
H	18-Jul-2012	Post ACS turn 21
J	29-Jul-2012	Post TCM-4

Once a baseline OD solution had been created, a large number of solution variations from the baseline were examined for every new data arc. These filter variations were collectively known as "filterloop", as multiple OD solution variations were calculated by automatically looping through many different changes to the filter setup. This was used to calculate a new solution to the model parameters. The details of these different filter cases changed and evolved significantly during the cruise to Mars. The details for particular phases of the mission will be discussed below. Briefly, depending on the specific phase of the mission and any upcoming events, the filter variations included varying SRP model *a priori* covariances, older SRP models, data variations (e.g., Doppler-only or range-only solutions), and TCM and other ΔV event covariance scaling. Particularly during the approach phase, the filterloop focus was on the effect of estimating or removing consider parameters such as Mars and Earth ephemerides, or media corrections (troposphere and ionosphere). While not all variations were realistic, they all helped to determine what was a plausible set of OD solutions for a given data cutoff. Even less realistic assumptions helped highlight sensitivities to data or specific model parameters.

4.1. Launch Support

The main objective for orbit determination during the launch phase was to enable successful reacquisition at the second complex at Madrid. The OD team processes tracking data from the first DSN complex at Canberra and creates a trajectory from which DSN antenna pointing and frequency shifts are derived.

The filter strategy and data weighting used for the MSL launch phase is shown in Tab. 4. Only a minimum set of parameters (state and range/Doppler biases) are estimated due to a limited amount of range and Doppler data available from a single tracking station. Furthermore, an *a priori* state constraint was applied based on a launch vehicle injection covariance provided by the launch vehicle manufacturer. In addition, the spin signature removal allowed OD to use a data weight reflecting the inherent accuracy of the tracking data. Initially, a Doppler bias was estimated to confirm the sign of the bias, which is determined by the polarization of the X-band signal. Once the correct polarization was confirmed, the *a priori* sigma on the Doppler bias was constrained, which significantly reduced the uncertainty of the trajectory solution.

The MSL injection was very accurate – better than the 0.5-sigma level of the pre-launch injection accuracy[2]. The accuracy of injection became evident after about 2 hours into flight as can be seen in Fig. 4, which shows the early trajectory solution history compared to the nominal pre-launch trajectory and uncertainty in terms of the right ascension (RA) of the outbound asymptote and C3. Two OD solutions were computed during launch with *a priori* state constraints of 10-times and 100-times the launch vehicle injection covariance. After 2 hours of tracking data, the two constraint solutions converged. For reference, the two horizontal dashed lines are the launch injection requirements.

Table 4: Launch Filter Setup

Data Type or Parameter	*A Priori* Uncertainty (1-σ)	Correlation Time	Update Time	Comments
Data Weights				
X-Band 2-way Doppler (mm/s)	1.776			0.1 Hz
Range (m)	5			
Bias Parameters				
Epoch state position X, Y, Z (km)	28.0, 33.1, 14.0			10 times full launch vehicle injection covariance
Epoch state velocity X, Y, Z (km/s)	0.04, 0.016, 0.045			10 times full launch vehicle injection covariance
Doppler bias (mm/s)	3.552			0.2 Hz (expected bias 0.074 Hz)
Consider Parameters				
Station locations	Full 2003 covariance			
Stochastic Parameters				
Parameter	***A Priori* Uncertainty (1-σ)**	**Correlation Time**	**Update Time**	**Comments**
Range bias (m)	2	0	Per pass	DSN performance

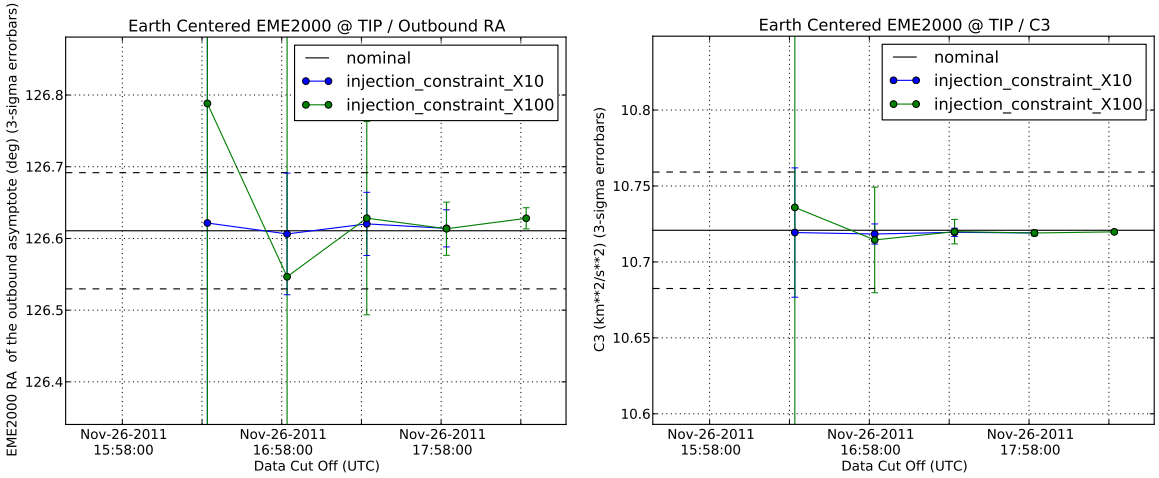

(a) Right Ascension (b) C3

Figure 4: Launch Solution

4.2. Early Cruise

After launch, the first objective was to calibrate the pre-launch dynamical models. For MSL, this learning period spanned from the second tracking pass to January 11, 2012. During early cruise, the MSL spacecraft experienced outgassing, which limited the ability to estimate the dynamical model parameters uniquely and accurately. The complete early cruise filter strategy is shown in Tab. 5. Any changes or new additions with respect to the launch phase filter strategy have been highlighted in blue.

For early cruise, estimation of Fourier coefficients of the MSL SRP model was added to the filter setup. The complete MSL SRP model is up to order 2, which means that 6 coefficient are used per spacecraft axis (3 cosine and 3 sine) resulting in 18 coefficients for the total SRP model. In the filter setup, 9 Fourier coefficients were estimated as bias parameters (see Tab. 5) and the zero order cosine coefficients for each spacecraft axis were estimated as stochastic parameters with only one update at the data cut off. The uncertainty of the three stochastic SRP parameters was reset at the data cut off to the *a priori* uncertainty and this uncertainty was mapped to Mars.

During cruise, the spacecraft attitude is changed occasionally to meet communication and thermal requirements. These turns are performed with the ACS thrusters, which may result in a net ΔV imparted on the spacecraft due to thruster imbalance. The estimation of the ACS turn ΔV per spacecraft axis was added to the filter setup as a small impulse ΔV bias parameter. To account for the uncertainty associated with future ACS turn ΔVs, the ACS turn ΔVs per spacecraft axis were added as consider parameters to the filter.

Table 5: Early Cruise Filter Setup

Data Type or Parameter	*A Priori* Uncertainty (1-σ)	Comments
Data Weights		
X-Band 2-way Doppler (mm/s)	0.053	3 mHz
Range (m)	2	
ΔDOR (ps)	60	About 2.4 nrad, for 3 points
Bias Parameters		
Epoch state position (km)	5.0e6	
Epoch state velocity (km/s)	5.0e3	
SRP X sine, N = 1,2 cosine N=1,2 (m^2)	1	Fourier coefficients of surface area
SRP Y sine, N = 1 (m^2)	1	Fourier coefficients of surface area
SRP Z sine, N=1,2, cosine, N = 1,2 (m^2)	1	Fourier coefficients of surface area
ACS Event ΔV (mm/s)	2	
Lateral calibration	–	8% proportional error and 5 mm/s fixed error (3-σ), vector mode maneuver.
Consider Parameters		
Station locations	Full 2003 covariance	
ACS event ΔV (mm/s)	2	For future ACS ΔV events only
Quasar locations (nrad)	0.5	

Stochastic Parameters				
Parameter	***A Priori* Uncertainty (1-σ)**	**Correlation Time**	**Update Time**	**Comments**
Range bias (m)	1	0	Per pass	DSN performance
SRP X,Y,Z cosine, N=0 (m^2)	1	0	At DCO	Uncertainty reset to a priori value at DCO, estimate propagated to Mars
Empirical exponential acceleration (km/s^2) apriori / process-noise	1.0e-11 / 1.0e-11	3 days	1 day	Outgassing model

After launch the MSL spacecraft experienced outgassing, which was modeled in the filter as a stochastic empirical exponential acceleration per spacecraft axis. It should be noted that the estimated SRP and outgassing models during early cruise did not represent an accurate representation due to high correlation between both dynamic models and relatively short data arcs.

During early cruise, a constant Doppler weight was used based on noise estimates after spin signature removal. The Doppler bias parameter estimate was removed from the filter setup because the spin signature and the Doppler bias were removed from the Doppler tracking data. The range measurement weight was increased to reflect the observed DSN performance. At the end of early cruise, the first ΔDOR measurements were taken, therefore the quasar locations were added to the filter setup as consider parameters and the recommended ΔDOR data weight was used (Jim Border, personal communication, 2012).

The official OD solutions and uncertainty ellipses for the early cruise phase are shown in Figs. 5a and 5b. Figure 5a shows the OD solutions with respect to the atmospheric entry target and the uncertainty corridor of 0.2° for the flight path angle in black. Figure 5b is a zoom in of Fig. 5a, showing the solutions after MSL injection and after the first maneuver to calibrate the lateral maneuver performance. The goal for the OD solutions is to be statistically consistent, which means that OD solution location changes in the B-plane are small compared to the contraction of the 3-sigma ellipses when more tracking data is included in the following OD solution. Thus, if the following OD solution location and 3-sigma uncertainty ellipse is encapsulated by the previous solution then the OD solutions are considered statistically consistent. If 3-sigma ellipses are not encapsulated then this is indicative of modeling error or overly optimistic uncertainty assumptions. In Fig. 5b, it should be noted that the solutions after injection are less statistically consistent. The reason for this is the outgassing experienced by the MSL spacecraft after launch. This occurred early in cruise, where OD models still needed to be calibrated and the time-varying behavior of the outgassing limited the accuracy of the OD solutions. At the time of the lateral calibration maneuver, the outgassing had subsided and the solutions became more statistically consistent as can be seen in Fig. 5b.

During early cruise, the filterloop variations were primarily focused on variations in the SRP model or dynamical models which could be incorrectly attributed to SRP (Fig. 6). Since the experience with the SRP model was limited at

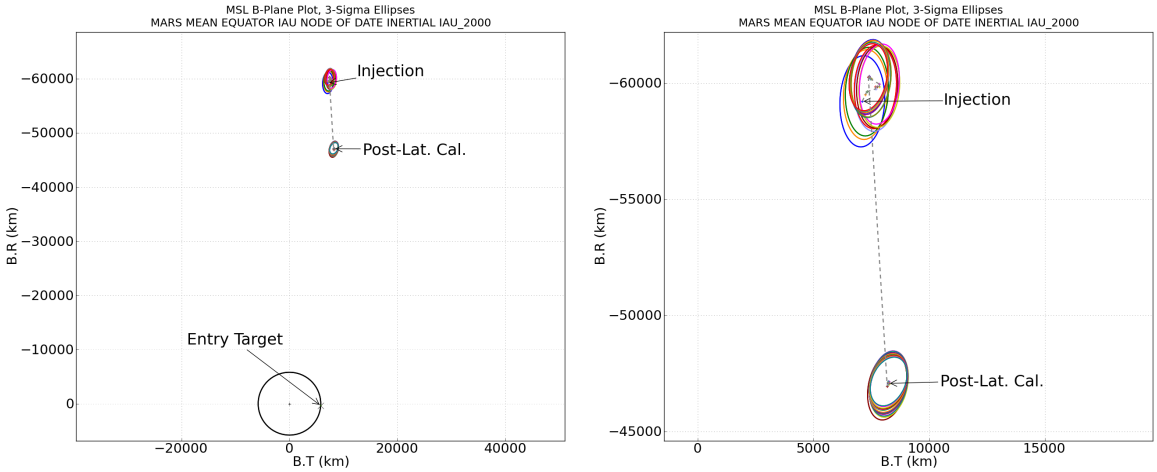

(a) Overview (b) Zoom on solutions

Figure 5: Early cruise B-plane

this time, the primary source of error mapped to the Mars B-plane was the assumed error at the time of a stochastic reset after the data cutoff (DCO). This was equivalent to considering this error source instead of estimating it, and was responsible for the large error ellipses shown in Fig. 6. These large ellipses include the baseline OD solution as well as variations in data types used and in the gas leak model used for the period soon after launch.

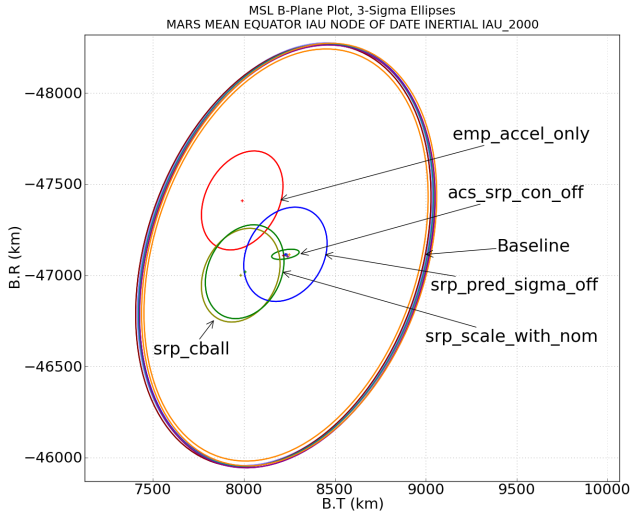

Figure 6: Early cruise filterloop

The other filterloop variations were attempts to significantly alter the SRP model. For example, there is one variation which removes the estimation of the individual SRP components and only estimates a single scale factor applied to the entire SRP model. Another example is to completely remove the SRP model parameters from the set of estimated parameters and introduce frequent, empirical, stochastic accelerations to fit the data arc; this is the solution to the upper-left of the baseline in the center. At this time, data variations or estimating some of the other consider parameters had no significant effect on the OD solution.

4.2.1. Outgassing Estimate Result

During the first few weeks the MSL spacecraft experienced outgassing, which had to be accommodated in the OD filter setup. In the early cruise period it was difficult to separate outgassing from other dynamical modeling errors due to the short orbit arcs of the OD solution and the time varying behavior of the outgassing. The outgassing result for the X, Y, and Z axes of the MSL spacecraft frame are shown in Fig. 7 for the final OD reconstruction of the complete

mission, which has the most accurate determination of the dynamical models, but correlations between some of the dynamical models remain. The results in Fig. 7 in general do show the expected exponential behavior of the outgassing, but variability can be seen for certain stochastic updates. Furthermore, Fig. 7 shows that the outgassing had subsided to very small levels in about two weeks after launch.

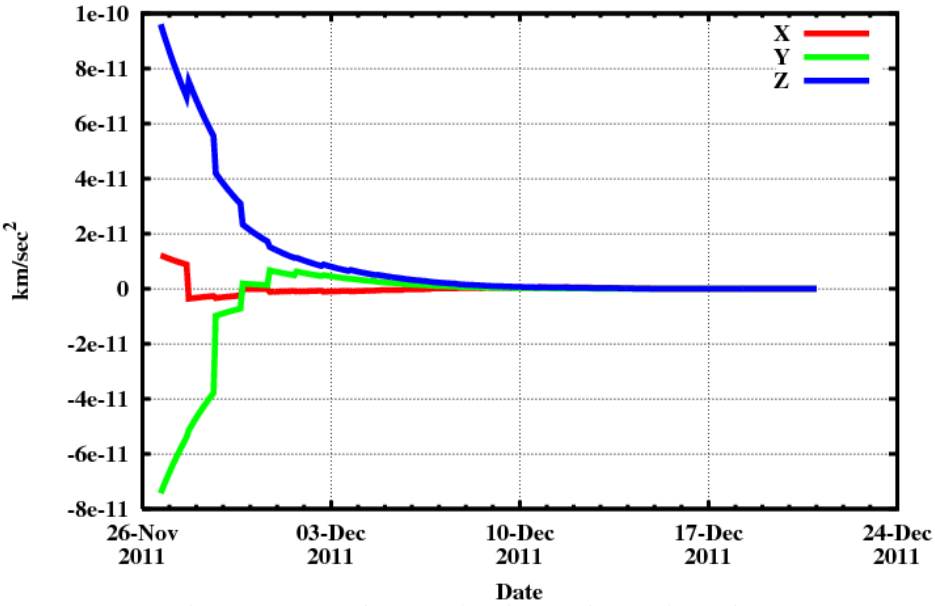

Figure 7: Outgassing Acceleration During Early Cruise

4.2.2. Lateral Maneuver Calibration

The MSL project decided to perform a lateral calibration maneuver (Lat. Cal.) before the large TCM-1 maneuver in order to verify the functionality of the propulsion system. The lateral calibration maneuver was executed on December 22, 2011, from 00:30:00 UTC to 00:50:00 UTC. The lateral calibration maneuver design was optimized with TCM-1, -2 and -3 to minimize propellant consumption [1]. The maneuver consisted of two lateral segments. In the OD filter, the lateral calibration maneuver design was used as *a priori* values and a constraint of 8% proportional and 5 mm/sec fixed error was applied in the solution. Furthermore, the individual ΔV estimates for each lateral segment were correlated in the a priori covariance assuming consistent ΔV behavior of the two lateral segments. Similar correlations were used for the RA and Dec estimates for all lateral segments. The lateral calibration reconstruction results, based on 19 days of DSN tracking data after the lateral calibration burn, are shown in Tab. 6. The overall lateral calibration had a ΔV magnitude error of 1.9% and a pointing error of 0.4°, which were well below the execution error assumptions.

Table 6: Lateral Calibration Results

Segment	Planned ΔV (m/s)	Estimated ΔV (m/s)	Estimated EME 2000 Right Ascension (deg)	Estimated EME2000 Declination (deg)	Estimated Propellant Usage (kg)	Magnitude Error (%)	Pointing Error (deg)
Lateral Segment 1	0.2790	0.2724	16.224	12.193	0.6410	2.386	0.150
Lateral Segment 2	0.2760	0.2726	16.314	12.608	0.6340	1.584	0.569
Total Lateral	0.5550	0.5450	16.269	12.401	1.2750	1.913	0.359

4.3. Mid-Cruise

The mid-cruise period encompasses the time interval from TCM-1 until TCM-2 execution. The emphasis for the OD team during this time period was the reconstruction of the TCM-1 maneuver and improving DSN Doppler and range tracking processing. For a complete overview of the mid-cruise filter setup see Tab. 7. Any changes or additions with respect to the early cruise filter strategy have been highlighted in blue.

During mid-cruise, the outgassing had subsided significantly, therefore the empirical exponential accelerations were removed from the mid-cruise filter setup. For the range bias estimation, a global range bias parameter *per station* was

Table 7: Mid-Cruise Filter Setup

Data Type or Parameter	*A Priori* Uncertainty (1-σ)	Comments
Data Weights		
X-Band 2-way Doppler (mm/s)	0.043	Per-pass weight floor, 60 second count time
Range (m)	1	Per-Pass weight floor
ΔDOR (ps)	60	About 2.4 nrad, for 3 points
Bias Parameters		
Epoch state position (km)	5.0e9	
Epoch state velocity (km/s)	5.0e6	
Station range bias (m)	2	Estimate per station over OD arc
SRP X sine, N = 1,2 cosine N=1,2 (m^2)	1	Fourier coefficients of surface area
SRP Y sine, N = 1 (m^2)	1	Fourier coefficients of surface area
SRP Z sine, N=1,2, cosine, N = 1,2 (m^2)	1	Fourier coefficients of surface area
ACS event ΔV (mm/s)	2	
Charged particle delay (range / Doppler)	1.5 m / 0.05 mm/s	Cubic spline updated daily
TCM-1	–	8% proportional error and 5 mm/s fixed error (3-σ), vector mode maneuver.
Consider Parameters		
Station locations	Full 2003 covariance	
ACS event ΔV (mm/s)	2	For future ACS ΔV events only
Quasar locations (nrad)	0.5	

Stochastic Parameters

Parameter	*A Priori* Uncertainty (1-σ)	Correlation Time	Update Time	Comments
Range bias (m)	1	0	Per pass	DSN performance
SRP X,Y,Z cosine, N=0 (m^2)	1	0	At DCO	Uncertainty reset to a priori value at DCO, estimate propagated to Mars

added to the filter setup and a stochastic range bias parameter *per-pass* was retrained to model per-pass range bias variations. The MSL flight occurred near a solar maximum which occasionally resulted in increased solar plasma density and noisy Doppler and range data. Daily charged particle delay cubic spline bias parameters were added to the filter setup to accommodate this noise source.

For mid-cruise, per-pass DSN tracking data weighting was introduced to appropriately weight passes with degraded data. The per-pass weights for Doppler and range were based on 3-sigma editing statistics of the post-fit residuals. The 3-sigma editing scheme uses an iterative approach where residuals are eliminated which deviate more than 3-sigma from the mean of the residuals of a pass. This process is repeated until no residual points are eliminated. If the 3-sigma derived data weight surpassed a specified ceiling then the ceiling weight was used in the OD filter process.

The official OD solutions for the mid-cruise phase, along with some late cruise solutions, are shown in Fig. 8a. The OD solution with the significantly larger uncertainty 3-sigma ellipse is the first OD solution after TCM-1 with only 30 minutes of tracking data after the completion of TCM-1. All other solutions show a decreasing uncertainty 3-sigma ellipses due to additional tracking data for each additional OD solution. The solution variations are small such that successive OD solution ellipses are encapsulated by the previous OD solution, which means the the OD solutions are statistically consistent under the uncertainty assumptions of the OD process. It should be noted in Fig. 8a that the uncertainty 3-sigma ellipses for final OD solutions are significantly smaller. For these solutions, the late cruise filter setup was adopted and these final OD solutions remain statistically consistent.

Figure 8b is showing the OD solution location for the C, D and E arcs. It should be noted in Fig. 8b that the OD solution locations were showing variations up to a few hundred km but after the adoption of the late cruise filter setup, the variations for different arcs were less than 50 km. The variations within one arc were even smaller at the 10-20 km level. Finally, the different orbit arc OD solution locations show systematic differences up to 50 km in Fig. 8b, but all these OD solutions are statistically consistent.

The filterloop variations for mid-cruise were still primarily designed to test variations and sensitivities to assumptions made for the SRP model as shown in Fig. 9. One of the key changes in the baseline OD assumptions was that the SRP model was updated. Along with this, the *a priori* error, and particularly the error post-DCO was significantly reduced.

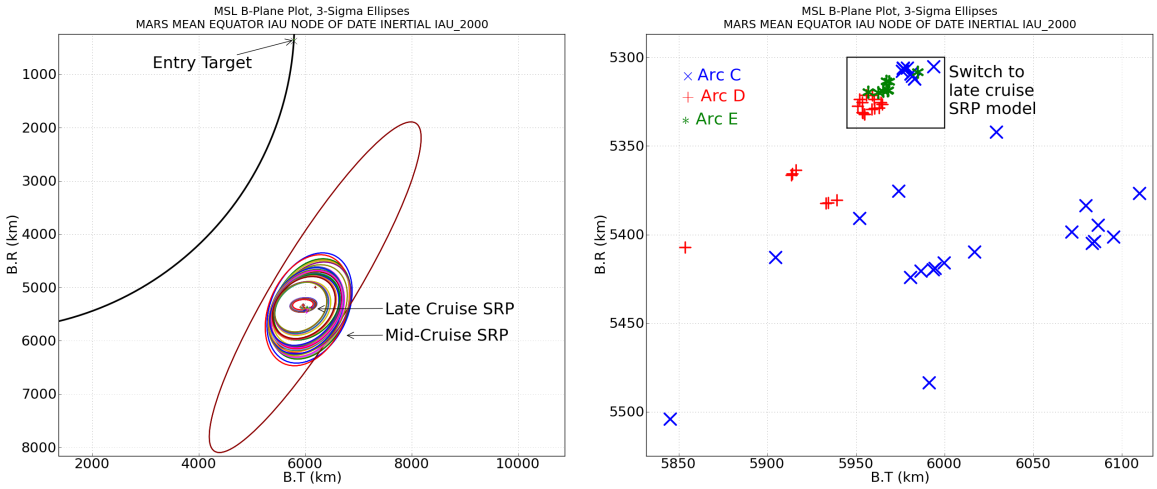

(a) TCM-1 to TCM-2 OD deliveries (b) TCM-1 to TCM-2 arc centers

Figure 8: Mid-Cruise and pre-TCM2 Late Cruise B-plane

In Fig. 9, there is one error ellipse which is larger than the others; it is the updated SRP model, but scaling the *a priori* error in the SRP parameters by a factor of three. Slightly smaller than that is the other ellipse which uses the older model. The baseline OD is in the cluster of smaller ellipses. As in early cruise, the primary source of error mapped to the future B-plane was due to the SRP model assumptions.

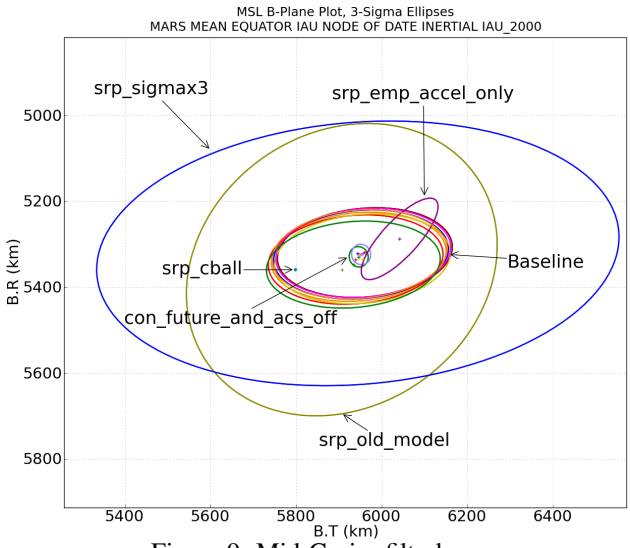

Figure 9: Mid-Cruise filterloop

Other variations which can be identified at this scale include the "srp_cball" SRP model which assumes the spacecraft is a homogenous sphere, and the "srp_emp_accel_only" which fixes the SRP model to the *a priori* model (removes it from set of estimated parameters) and uses empirical, stochastic accelerations to fit the data. Harder to identify are the filterloop variations which use selected data types (e.g., Doppler only), or delete the error in future events such as ΔV due to ACS turns. The primary conclusion at the time was that even for significant departures from the OD baseline assumptions, the filterloop variations were still statistically consistent with the baseline OD.

4.3.1. TCM-1

TCM-1 was executed between January 11, 2012 23:00:00 UTC and January 12 02:00:00 UTC. The TCM-1 was designed to remove most of the injection bias as part of a TCM-1, -2 and -3 optimization maneuver design scheme

[1]. The TCM-1 burn was executed in vector mode with an axial burn in the -Z axis and a lateral burn divided into 9 segments. In the OD filter, the TCM-1 maneuver design was used as *a priori* values and a constraint of 8% proportional and 5 mm/sec fixed error was applied in the solution. Furthermore, the individual ΔV estimates for each lateral segment were correlated in the *a priori* covariance assuming consistent ΔV behavior of all lateral segments. The correlation was added to the covariance due to the lack of observability of each lateral segment ΔV. Similar correlations were used for the RA and Dec estimates for all lateral segments. The TCM-1 reconstruction results by the OD team are shown in Tab. 8 based on 19 days of DSN tracking data after the TCM-1 burn. Overall, TCM-1 had a ΔV magnitude error of 2.3% and a pointing error of 0.6°, which were well below the execution error assumptions.

Table 8: TCM-1 Results

Segment	**Planned ΔV (m/s)**	**Estimated ΔV (m/s)**	**Estimated EME 2000 Right Ascension (deg)**	**Estimated EME2000 Declination (deg)**	**Estimated Propellant Usage (kg)**	**Magnitude Error (%)**	**Pointing Error (deg)**
Minus Z Axial Burn	1.5853	1.6527	286.696	14.979	4.6619	4.249	0.022
Lateral Segment 1	0.7484	0.7631	167.662	39.253	1.7773	1.973	0.527
Lateral Segment 2	0.7304	0.7457	167.478	39.196	1.7366	2.102	0.437
Lateral Segment 3	0.7138	0.7292	167.400	39.177	1.6988	2.159	0.415
Lateral Segment 4	0.6984	0.7138	167.348	39.167	1.6647	2.199	0.408
Lateral Segment 5	0.6842	0.6996	167.283	39.151	1.6307	2.248	0.403
Lateral Segment 6	0.6710	0.6862	167.253	39.148	1.6004	2.273	0.406
Lateral Segment 7	0.6586	0.6738	167.199	39.136	1.5724	2.315	0.410
Lateral Segment 8	0.6470	0.6622	167.173	39.134	1.5441	2.337	0.417
Lateral Segment 9	0.0593	0.0610	166.472	38.846	0.1449	2.790	0.740
Total Lateral	5.6111	5.7346	167.347	39.169	13.3698	2.201	0.410
Total TCM-1	5.5071	5.6350	188.146	45.937	18.0317	2.323	0.618

4.3.2. ACS/NAV Thruster Calibration

The objective of the ACS/NAV calibration was to characterize the residual translational ΔV produced by spacecraft turns. A spacecraft turn uses pairs of thrusters firing in opposite directions, so it nominally produces zero net ΔV, but because thrusters in general are not perfectly balanced, a small ΔV will be produced. The ACS/NAV calibration consisted of two identical sets of four 4.5° turns that are representative of the spacecraft turns performed during late cruise and approach. The ACS/NAV calibration was initiated by a turn such that the angular momentum vector of the spacecraft was about 40° away from the line of sight vector. One set consisted out four 4.5° turns. The first two turns are away and towards the line of sight vector in a plane containing the line of sight vector and the angular momentum vector prior to the 4.5° turns. The last two turns are perpendicular to the plane of the first two turns. One set of turns provides sufficient independent line of sight ΔV measurements to uniquely determine the total ΔV vector for a 4.5° turn. Two sets of turns were executed to assess repeatability of the estimated turn ΔV.

The ACS/NAV calibration was successfully executed on January 25, 2012. The line of sight ΔV changes were small, as can be seen in Fig. 10, which shows the two-way Doppler residuals during the ACS/NAV cal. The line of sight ΔVs varied from between 0 and 8 mHz (0.16 mm/sec). The total turn ΔVs were estimated in inertial frames that coincide with mean position of the spacecraft coordinate frame axes during a turn. This allows for a direct comparison between the individual ΔV estimates per turn, since each estimate can be interpreted as being within the spacecraft coordinate frame. The results of the combined ΔV estimates is shown in Tab. 9. This table shows the results as ΔV per axis per degree to facilitate the calculation of turn ΔVs that are not 4.5°. The results show only small ΔVs and excellent repeatability over the 8 turns during the ACS/NAV cal. The results in Tab. 9 were used as the bases for future ACS turn ΔV prediction in the orbit determination filter setup.

Table 9: ACS/NAV Calibration Results Expressed in the MSL ACS Turn Frame

	X (mm/s/deg)	**Y (mm/s/deg)**	**Z (mm/s/deg)**
Mean	0.002271	0.024250	-0.023118
Sigma	0.005	0.005	0.005

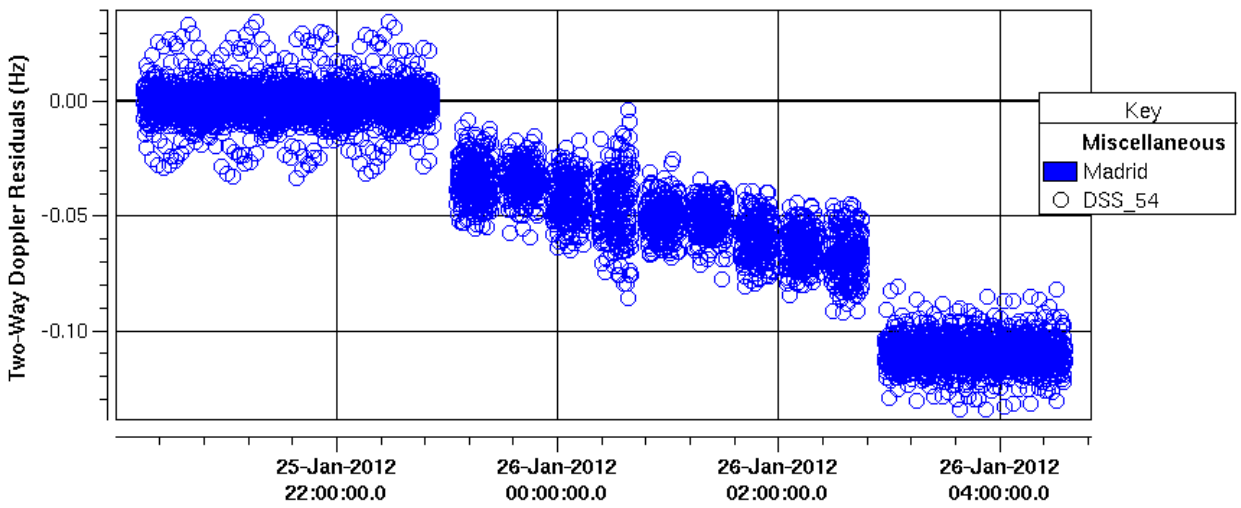

Figure 10: ACS/NAV Calibration Doppler Residuals

4.4. Late Cruise

The late cruise period started on March 5, 2012, and concluded at TCM-4. During this period, the OD team focused on calibration and improvement of the dynamic models and their associated uncertainties. TCM-2 and 3 were reconstructed as well. For a complete overview of the late cruise filter setup see Tab. 10. Any changes or additions with respect to the late cruise filter strategy have been highlighted in blue.

At the end of mid-cruise, the 12 parameters of the MSL SRP model did not fit the ΔDOR measurement well compared to similar fits for the Mars Exploration Rovers (MER) for the whole mission. This is because MSL has an RTG onboard, which introduces a net thermal radiation acceleration in the direction of the rotation axis (Z-axis) of the MSL spacecraft. Furthermore, this thermal radiation is independent from the distance to the Sun and solar flux. Thus, the 12 parameter SRP model used in mid-cruise was unable to correctly model SRP and the thermal acceleration. Two SRP model changes were made to the late cruise filter setup. First, the MSL SRP was augmented with a stochastic acceleration in the Z-axis to estimate the thermal radiation acceleration. Second, the number of Fourier coefficients estimated was reduced to only three bias parameters because these three coefficients modeled SRP accurately given the relatively small range of solar colatitudes the MSL spacecraft experienced during this phase. This change also significantly reduced the B-plane 3-sigma uncertainty ellipses for the OD solutions (see Fig. 8a). This reduction was caused by the estimation of only 3 instead of 12 SRP model parameters and the removal of the stochastic reset, to the *a priori* uncertainty values, of three SRP Fourier coefficients at the OD arc data cut off.

As the late cruise progressed, it became clear that the ACS turn ΔV kept decreasing with each ACS turn. To model this decrease, a stochastic ACS turn ΔV scale factor was added to the filter setup. The last stochastic update prior to the data cutoff was then applied to all future ACS turns in the trajectory and uncertainty propagation to Mars.

Additional consider parameters were added to the filter setup: Earth polar motion, Earth length of day, day and night ionospheric delays, wet and dry tropospheric delays, Mars and Earth ephemerides, and the Mars gravity parameter GM.

The official OD solutions and uncertainty ellipses for the late cruise phase after TCM-2 are shown in Figs. 11a and 11c. Figure 11a shows the official OD solutions between TCM-2 and TCM-3 and Fig. 11c shows the OD solutions between TCM-3 and TCM-4. Initially both Figs. 11a and 11c show larger 3-sigma uncertainty ellipses after the maneuver until the the first couple of ΔDOR measurements have been included in the OD solution, however all solutions are statistically consistent. Figure 11b shows the OD locations in the B-plane for the C, D, E and F OD arcs. Figure 11d additionally shows arcs G and H. Most OD solution variations are within 50 km and all these OD solution locations are statistically consistent, even though systematic difference exist. Figure 11 also shows the 0.2° uncertainty flight path angle uncertainty corridor in black. Furthermore, the green and yellow TCM-5 decision criteria box described in

Table 10: Late Cruise Filter Setup

Data Type or Parameter	*A Priori* Uncertainty (1-σ)	Comments
Data Weights		
X-Band 2-way Doppler (mm/s)	0.043	Per-pass weight floor, 60 second count time
Range (m)	1	Per-pass weight floor
ΔDOR (ps)	60	About 2.4 nrad, for 3 points
Bias Parameters		
Epoch state position (km)	1000	
Epoch state velocity (km/s)	1.0	
Station range bias (m)	2	Estimate per station over OD arc
SRP X sine, N = 1 (%)	5	Fourier coefficients, percentage of frontal area of 26 m^2
SRP Y sine, N = 1 (%)	1	Fourier coefficients, percentage of frontal area of 26 m^2
SRP Z cosine, N = 1 (%)	5	Fourier coefficients, percentage of frontal area of 26 m^2
ACS event ΔV (8° turn) (mm/s)	0.04	0.005 mm/s/deg
Charged particle delay (range / Doppler)	1.5 m / 0.05 mm/s	Cubic spline updated daily
TCM-2	–	5% proportional error and 4 mm/s fixed error (3-σ), vector mode maneuver.
TCM-3	–	5% proportional error and 4 mm/s fixed error (3-σ), vector mode maneuver.
Consider Parameters		
Station locations	full 2003 covariance	
ACS event ΔV (8° turn) (mm/s)	0.04	0.005 mm/s/deg, future ACS events
Quasar locations (nrad)	0.5	
Pole X, Y (cm)	0.5	
UT1 (cm)	3.67	
Ionosphere day / night (cm)	55 / 15	
Troposphere wet / dry (cm)	1 / 1	
Mars and Earth ephemerides	DE423 covariance	DE425 used in OD
Mars GM (km^3/s^2)	2.80e-04	About 10 times MGS95J formal error

Stochastic Parameters				
Parameter	***A Priori* Uncertainty (1-σ)**	**Correlation Time**	**Update Time**	**Comments**
Range bias (m)	1	0	Per pass	DSN performance
Z thermal acceleration (km/s^2) apriori / process-noise	8e-13 / 4e-13	30 days	7 days	Model radiated heat from RTG
ACS turn ΔV scale factor apriori / process-noise	0.3 / 0.3	30 days	7 days	X: 0.002 mm/s/deg, Y, Z: 0.020 mm/s/deg

Section 1 are shown, illustrating the need for executing TCM-3 (Fig. 11b) and TCM-4 (Fig. 11d).

With less time remaining in the mission, and with extensive experience with the SRP model, the error in the SRP model no longer dominated all other effects when mapping to the B-plane (Fig. 12). While difficult to see at this scale, all of the plausible OD solutions from the filterloop variations are tightly clustered in the center of the error ellipses. What is illustrated at this larger scale is what occurs due to using different data variations. For example, Doppler-only, Doppler and range-only, Doppler and ΔDOR-only. Even just using only the North-South or East-West ΔDOR baselines were analyzed although none of these were considered plausible or realistic OD solutions. At this scale, filterloop results highlight the sensitivities to the data as well as some of the dynamic model assumptions.

As can be seen in Fig. 12, all of the larger error ellipses are due to different data variations. Every data type used – Doppler, range, ΔDOR– was critical to achieving the most precise OD solution. There are a large number of other filterloop variations all clustered tightly inside the larger error ellipses. This points to the stability of the OD relative to assumptions made about the SRP model, considering vs. estimating parameters (e.g., media calibrations), data arc length, thermal acceleration due to the RTG, and data weights. None of these variations significantly altered the baseline OD trajectory or covariance.

4.4.1. ACS Turn ΔV Trending

During mid-cruise the estimated ACS turn ΔV decreased in magnitude, which led to the filter setup change discussed in the previous section. The filter setup change was made to improve the predictability of the ACS turn ΔV, which directly

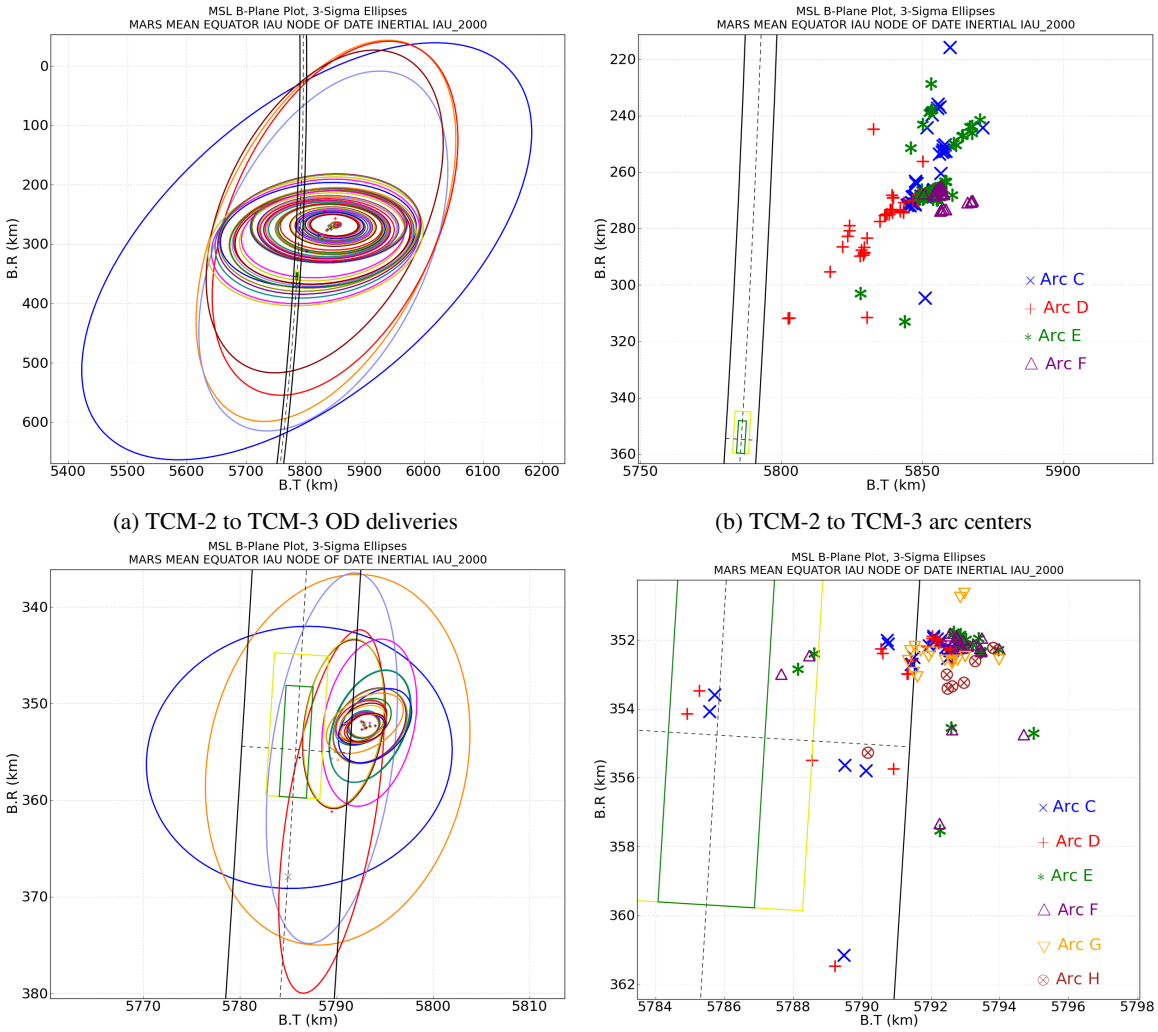

(a) TCM-2 to TCM-3 OD deliveries

(b) TCM-2 to TCM-3 arc centers

(c) TCM-3 to TCM-4 OD deliveries

(d) TCM-3 to TCM-4 arc centers

Figure 11: Late Cruise B-plane

affected the predicted B-plane location at Mars and the associated uncertainty. The ACS turn ΔV scale factor scales the ACS/NAV calibration results shown in Tab. 9, which were used during the mission to predict the ACS turn ΔV for future turns. Figure 13 shows the estimated ACS turn ΔV scale vector history for the final trajectory reconstruction of the complete mission. Initially the ACS turn ΔV changed significantly (over 50%), but in late cruise started to stabilize at a slower decay rate improving the predictably of the ACS turn ΔV.

4.4.2. TCM-2

TCM-2 was executed on March 26, 2012, from 19:00:00 UTC to 19:50:00 UTC. TCM-2 was targeted directly to the Gale Crater atmospheric interface because of the excellent injection of the spacecraft and successful TCM-1 execution. Furthermore, direct targeting did not violate planetary protection requirements. TCM-2 was executed in vector mode with an axial burn in the -Z axis and one lateral burn segment. In the OD filter, the TCM-2 maneuver design was used as *a priori* values and a constraint of 5% proportional and 4 mm/sec fixed error was applied in the solution. The TCM-2 reconstruction results, based on 38 days of DSN tracking data after the burn are shown in Tab. 11. The overall TCM-2 ΔV magnitude error was 0.04% and a pointing error of 0.4°, which was well below the execution error assumption.

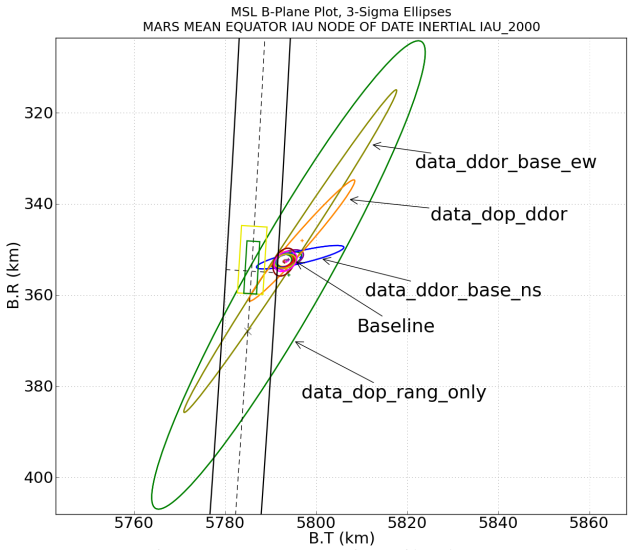

Figure 12: Late Cruise Filterloop

Table 11: TCM-2 Results

Segment	Planned ΔV (m/s)	Estimated ΔV (m/s)	Estimated EME 2000 Right Ascension (deg)	Estimated EME2000 Declination (deg)	Estimated Propellant Usage (kg)	Magnitude Error (%)	Pointing Error (deg)
Minus Z Axial Burn	0.1954	0.1980	311.871	-11.700	0.5421	1.334	0.001
Lateral Segment 1	0.7265	0.7270	218.150	67.778	1.6852	0.069	0.385
Total TCM-2	0.7116	0.7119	254.555	62.747	2.2273	0.038	0.388

4.4.3. TCM-3

TCM-3 was executed on June 26, 2012, from 17:00:00 UTC to 17:40:00 UTC. Like TCM-2, TCM-3 was also targeted to the Gale Crater atmospheric interface. TCM-3 was executed in vector mode with an axial burn in the -Z axis and one lateral burn segment. In the OD filter, the TCM-3 maneuver design was used as a *a priori* values and a constraint of 5% proportional and 4 mm/sec fixed error was applied in the solution. The TCM-3 reconstruction results, based on 21 days of DSN tracking data after the maneuver, are shown in Tab. 12. Overall, TCM-3 had a ΔV magnitude error of 1.0% and a pointing error of 2.5°, which were well below the execution error assumptions.

Table 12: TCM-3 Results

Segment	Planned ΔV (m/s)	Estimated ΔV (m/s)	Estimated EME 2000 Right Ascension (deg)	Estimated EME2000 Declination (deg)	Estimated Propellant Usage (kg)	Magnitude Error (%)	Pointing Error (deg)
Minus Z Axial Burn	0.028	0.029	174.449	2.176	0.079	4.576	1.231
Lateral Segment 1	0.026	0.025	242.983	-52.453	0.059	-2.078	0.630
Total TCM-3	0.041	0.042	196.836	-26.702	0.138	1.029	2.462

4.5. Final Approach

The final approach phase started at TCM-4 and ended with the MSL spacecraft reaching the Mars atmospheric entry interface. Towards the end of late cruise, the late cruise filter setup was only tweaked by reducing the uncertainty for two SRP Fourier coefficients and the stochastic acceleration in the MSL Z-axis. The complete filter setup for final approach is shown in Tab. 13. Any changes or additions with respect to the mid-cruise filter strategy have been highlighted in blue.

The official OD solutions and uncertainty ellipses for the final approach are shown in Fig. 14a. All solutions between TCM-4 through 40 minutes before entry are shown. The OD solutions were statistically consistent and also very stable as can be seen in Fig. 14b for the F, G, H and J arcs. The OD solution used for the first entry parameter update (EPU-1)

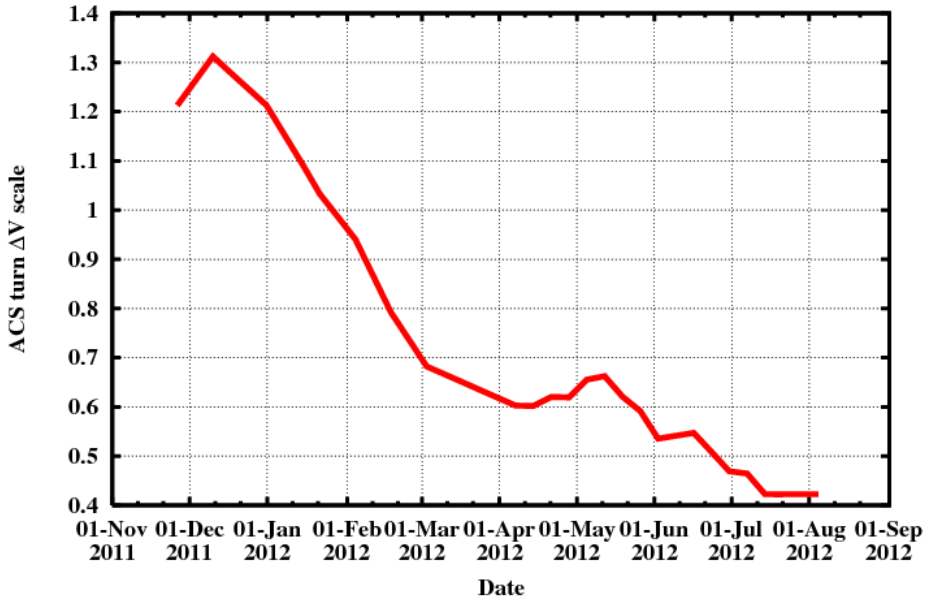

Figure 13: ACS turn ΔV scale

was based on tracking data up to Entry-6.5 days. Since the OD solutions were so stable with variations less than 400 m in the B-plane, the MSL project decide to waive the remaining three planned updates after EPU-1. The EPU-1 solution is shown along with the final OD solution in Fig. 14b. The final solution is the most accurate and it turned out to be separated about 200 m from EPU-1 in the B-plane. The accurate prediction of EPU-1 can be attributed to proper calibration of the dynamical models for the MSL spacecraft and the relatively low noise in the first two ΔDOR measurements after TCM-4 used in the EPU-1 OD solution. The OD solutions after EPU-1 did jump around at the few 100-meter level, mainly due to noise in the ΔDOR measurements and media calibration updates for the DSN tracking data.

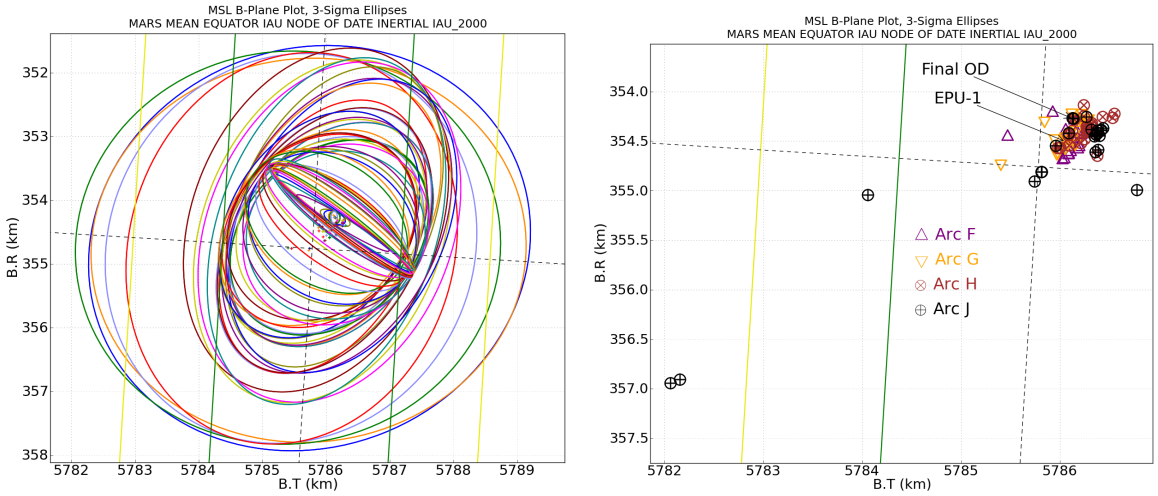

(a) TCM-4 to Entry OD deliveries

(b) TCM-4 to Entry arc centers

Figure 14: Final approach B-plane

During the final approach, the OD solutions were very stable. As in the late cruise period, one of the primary contributions of filterloop was to help illustrate the sensitivities to specific data types, e.g., ΔDOR. The primary sources of error were consider effects, including the errors in Earth ephemeris, Mars ephemeris, Earth polar motion and length

Table 13: Final Approach Filter Setup

Data Type or Parameter	*A Priori* Uncertainty (1-σ)	Comments
Data Weights		
X-Band 2-way Doppler (mm/s)	0.043	Per-pass weight floor, 60 second count time
Range (m)	1	Per-pass weight floor
ΔDOR (ps)	60	About 2.4 nrad, for 3 points
Bias Parameters		
Epoch state position (km)	1000	
Epoch state velocity (km/s)	1.0	
Station range bias (m)	2	Estimate per station over OD arc
SRP X sine, N = 1 (%)	2	Fourier coefficients, percentage of frontal area of 26 m^2
SRP Y sine, N = 1 (%)	1	Fourier coefficients, percentage of frontal area of 26 m^2
SRP Z cosine, N = 1 (%)	2	Fourier coefficients, percentage of frontal area of 26 m^2
ACS event ΔV (8° turn) (mm/s)	0.04	0.005 mm/s/deg
Charged particle delay (range / Doppler)	1.5 m / 0.05 mm/s	Cubic spline updated daily
TCM-4	–	5% proportional error and 4 mm/s fixed error (3-σ), vector mode maneuver.
Consider Parameters		
Station locations	Full 2003 covariance	
ACS event ΔV (8° turn) (mm/s)	0.04	0.005 mm/s/deg, future ACS events
Quasar locations (nrad)	0.5	
Pole X, Y (cm)	0.5	
UT1 (cm)	3.67	
Ionosphere day / night (cm)	55 / 15	
Troposphere wet / dry (cm)	1 / 1	
Mars and Earth ephemerides	DE423 covariance	DE425 used in OD
Mars GM (km^3/s^2)	2.80e-04	About 10 times MGS95J formal error

Stochastic Parameters

Parameter	*A Priori* Uncertainty (1-σ)	Correlation Time	Update Time	Comments
Range bias (m)	1	0	Per pass	DSN performance
Z thermal acceleration (km/s^2) apriori / process-noise	3e-12 / 1e-13	30 days	7 days	Model radiated heat from RTG
ACS turn ΔV scale factor apriori / process-noise	0.3 / 0.3	30 days	7 days	X: 0.002 mm/s/deg, Y, Z: 0.020 mm/s/deg

of day, and tropospheric and ionospheric (media) calibrations. There are approximately 40 different filterloop variations represented in Fig. 15a, combining all the different variations used during the different mission phases. The first thing to note is how stable the OD is relative to all the different filter variations studied.

Second, the dominant error contributions as shown by filterloop were due to considering the media effects. This is better illustrated in Fig. 15b. Shown here are the baseline OD and 3 variations to the media uncertainty: complete removal of the error (con_media_remove), estimation as a bias (con_media_bias), and estimation as a stochastic (con_media_stoch). Either removing the error completely or estimating it has the same effect on the covariance: a reduction in the size of the error ellipse. However, note that the OD trajectory depends on whether the estimate is done as bias or stochastic parameters. This is not to say that it would be appropriate to estimate these as a bias, only that any undetected bias in the media calibrations would affect the solution in this way.

4.5.1. TCM-4

TCM-4 was executed on July 29, 2012 05:00:00 UTC as a lateral burn only, which resulted in a slight targeting offset in the B-plane and about 2-second difference in arrival time. However, these small changes were well within the desired B-plane green box shown the in Fig. 14a. In the OD filter, the TCM-4 maneuver design was used as *a priori* values and a constraint of 5% proportional and 4 mm/sec fixed error was applied in the solution. The TCM-4 reconstruction, based on 5.5 days of DSN tracking data after the maneuver, is shown in Tab. 14. Overall, TCM-4 had a ΔV magnitude error of 5.7% and a pointing error of 1.8°. For small burns, the fixed error is the dominant term, so the execution error of TCM-4 appears larger as a percentage when compared to previous, larger burns. In absolute terms, the ΔV error was about 1 mm/sec, which is well below the fixed error assumption.

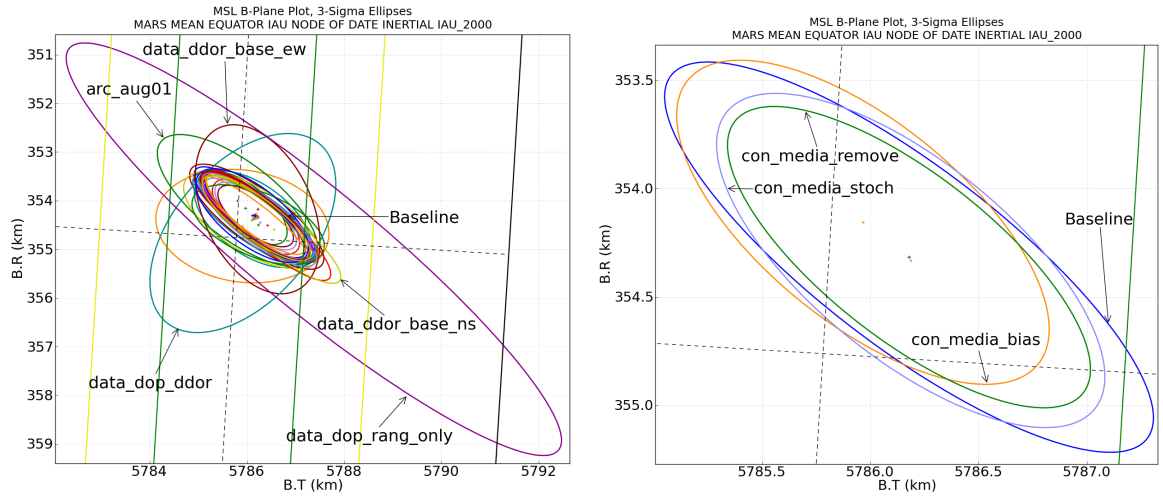

(a) Filterloop (b) Media filterloop

Figure 15: Final approach filterloop

Table 14: TCM-4 Results

Segment	Planned ΔV (m/s)	Estimated ΔV (m/s)	Estimated EME 2000 Right Ascension (deg)	Estimated EME2000 Declination (deg)	Estimated Propellant Usage (kg)	Magnitude Error (%)	Pointing Error (deg)
Lateral Segment 1	0.0111	0.0104	266.504	-44.659	0.026	-5.702	1.750

TCM-5 was canceled because of a successful TCM-4 execution and the stability of the OD solutions after the TCM-4 execution, which were within the desired B-plane green box shown the in Fig. 14a.

4.5.2. Full-Mission Reconstruction

After Curiosity landed, the OD team performed a full reconstruction of the entire mission. Figures 16 through 18 show the converged pre-fit residuals, which are computed with respect to the converged trajectory without correcting for the estimates of charged particles delays or range biases. A clear example of increased solar activity can be seen in Figs. 16 and 17 in early March – note the multiple-pass trending. The large residuals in Fig. 16 during TCMs are because a lower compression time was used, which results in increased noise. The dramatic range noise reduction on February 28, 2012, seen in Fig. 17, is due to the switch from the LGA to the MGA. Over the entire mission, the residual standard deviations for Doppler, range and ΔDOR were: 1.1×10^{-3} Hz, 8.6 RU,[1] and 35.7×10^{-11} sec, respectively.

5. Conclusion

The MSL orbit determination was very successful and enabled the very precise landing of the Curiosity rover in Gale Crater on Mars. Throughout cruise, the orbit determination met all requirements with a considerable margin. The MSL OD team developed a spin signature removal tool, which successfully removed the spin signature and bias from the Doppler and range data. A novel approach was successfully used for modeling the SRP via a Fourier expansion of the net solar radiation force. The SRP model evolved into a highly accurate model by estimation of only 3 Fourier coefficients. Additionally, a stochastic acceleration in the direction of the rotation axis was used to model thermal radiation from the RTG. All trajectory correction maneuvers were successfully reconstructed and execution errors were found to be less than the assumed execution errors pre-flight. The ΔVs associated with ACS turns were successfully calibrated in the beginning of the mission, but a decrease in ΔV magnitude was observed as cruise progressed. A stochastic scale factor for the ASC turn ΔV was estimated, which significantly improved the ΔV prediction accuracy for future ACS turns. For each cruise phase, the OD solutions showed statistical consistency as more tracking was included in the solution. Small systematic differences could be seen between solutions from different OD arc lengths but these differences were well within the 3-sigma B-plane uncertainties.

[1] Range Units: 1 RU = 0.142 m

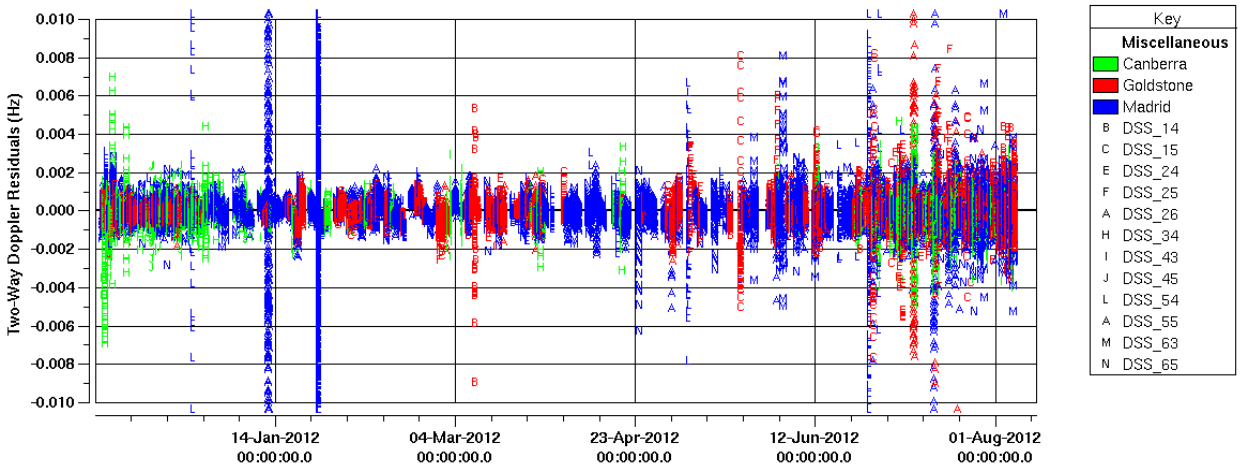

Figure 16: Doppler residuals for entire mission

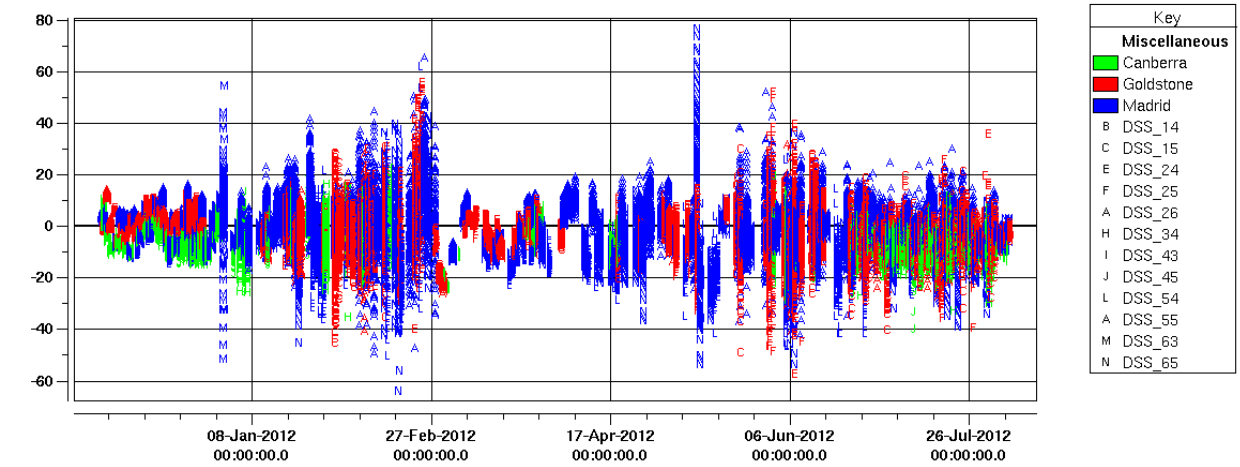

Figure 17: Range residuals for entire mission in RU

During final approach, the OD team provided one update (EPU-1) for the onboard entry state to be used by the entry guidance system. The OD solutions after EPU-1 were stable enough for the remaining the planned EPUs to be canceled. The final reconstructed trajectory differed from the EPU-1 trajectory by only about 200 m in the B-plane.

Acknowledgments

The orbit determination team could not have done our work without the other members of the JPL MSL navigation team. We would like to acknowledge the maneuver design team: Mau Wong (lead), Chris Ballard and Julie Kangas; Fernando Abilleira (cruise and relay analyst); the EDL trajectory team: Dan Burkhart (lead) and Jordi Casoliva; our shift leads: Allen Halsell and Tim McElrath; Jim Border (ΔDOR analyst); dedicated launch despinners: Matthew Abrahamson and Shadan Ardalan; our systems administrators: Jae Lee, Jason Bailey, Dimitrios Gerasimatos, Dan Jamerson, and Katherine Nakazono; and our EDL colleagues from JPL, Langley Research Center and Johnson Spaceflight Center. We also acknowledge the support we received from our section (Mission Design and Navigation) throughout development and flight of the MSL mission. The MONTE software was critical to our success, and we are very grateful to the development team for their support during the mission. We also want express our gratitude to the members of the Navigation Advisory Group, lead by Joe Guinn, for their constructive suggestions and advice during cruise. The success of the MSL orbit determination was facilitated by the excellent tracking data quality and support from the DSN. Navigators cannot leave Earth without them. Finally, we want to acknowledge our colleagues from Radio-Metric Data Conditioning (RMDC): K.J. Lee, Teresa Thomas and Kaye Olinarez for their excellent tracking data processing support

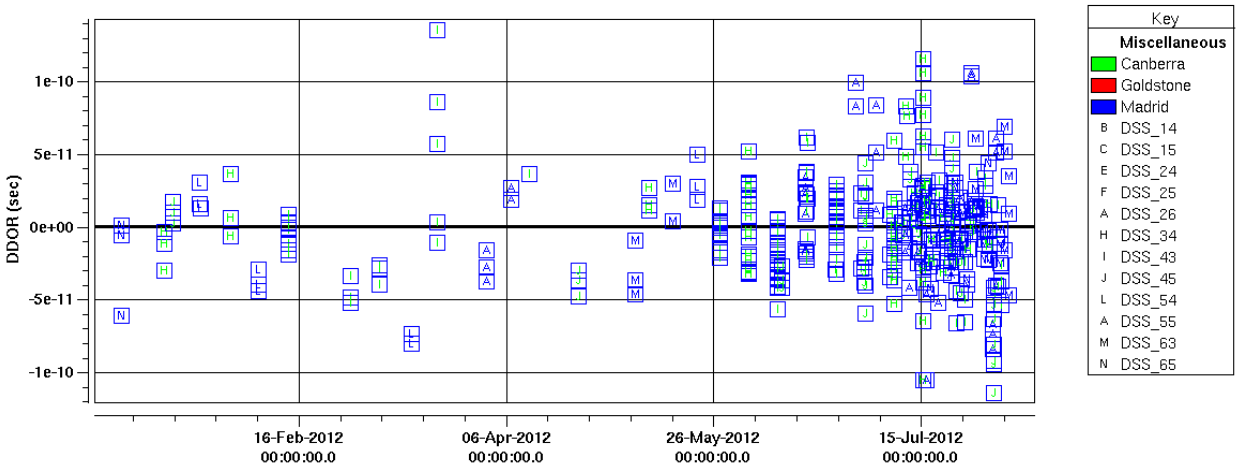

Figure 18: ΔDOR residuals for entire mission

during critical events.

This research was carried out at the Jet Propulsion Laboratory, California Institute of Technology, under a contract with the National Aeronautics and Space Administration. Reference herein to any specific commercial product, process or service by trade name, trademark, manufacturer, or otherwise, does not constitute or imply its endorsement by the United States Government or the Jet Propulsion Laboratory, California Institute of Technology.

6. References

[1] Wong, M. C., Kangas, J. A., Ballard, C. G., Gustafson, E. D., and Martin-Mur, T. J. "Mars Science Laboratory Propulsive Maneuver Design and Execution." 23rd International Symposium on Space Flight Dynamics. Pasadena, CA, USA, 2012.

[2] Martin-Mur, T. J., Kruizinga, G. L., Burkhart, P. D., Wong, M. C., and Abilleira, F. "Mars Science Laboratory Navigation Results." 23rd International Symposium on Space Flight Dynamics. Pasadena, CA, USA, 2012.

[3] Sunseri, R. F., Wu, H.-C., Evans, S. E., Evans, J. R., Drain, T. R., and Guevara, M. M. "Mission Analysis, Operations, and Navigation Toolkit Environment (Monte) Version 040." NASA Tech Briefs, Vol. 45, September 2012.

[4] Folkner, W. M. "Planetary Ephemeris DE424 for MSL Early Cruise Navigation, IOM 343R-11-003." JPL Inter-Office Memorandum, 2011.

[5] Folkner, W. M. "Planetary Ephemeris DE425 for Mars Science Laboratory Arrival, IOM 343R-12-002." JPL Inter-Office Memorandum, 2012.

[6] Folkner, W. M. "Planetary Ephemeris DE423 Fit to MESSENGER Encounters with Mercury, IOM 343R-10-001." JPL Inter-Office Memorandum, 2010.

[7] Abilleira, F. "Mars Science Laboratory Planetary Constants and Models Document." JPL D-27212, MSL-377-0316, October 2008.

[8] Tapley, B., Ries, J., Bettadpur, S., Chambers, D., Cheng, M., Condi, F., Gunter, B., Kang, Z., Nagel, P., Pastor, R., Pekker, T., Poole, S., and Wang, F. "GGM02 An Improved Earth Gravity Field Model from GRACE." Journal of Geodesy, Vol. 79, pp. 467–478, Nov. 2005. doi:10.1007/s00190-005-0480-z.

[9] Konopliv, A. S., Asmar, S. W., Carranza, E., Sjogren, W. L., and Yuan, D. N. "Recent Gravity Models as a Result of the Lunar Prospector Mission." Icarus, Vol. 150, pp. 1–18, Mar. 2001. doi:10.1006/icar.2000.6573.

[10] Konopliv, A. S., Yoder, C. F., Standish, E. M., Yuan, D.-N., and Sjogren, W. L. "A Global Solution for the Mars Static and Seasonal Gravity, Mars Orientation, Phobos and Deimos Masses, and Mars Ephemeris." Icarus, Vol. 182, pp. 23–50, May 2006. doi:10.1016/j.icarus.2005.12.025.

[11] Rubincam, D. P. "Yarkovsky Thermal Drag on LAGEOS." Journal of Geophysical Research, Vol. 93, No. B11, pp. 13805–13810, 1988. doi:10.1029/JB093iB11p13805.

[12] Petit, G. and Luzum, B., editors. IERS Conventions (2010) (IERS Technical Note 36). Frankfurt am Main: Verlag des Bundesamts für Kartographie und Geodäsie, 2010.

[13] Sniffin, R. W. 301, Rev. G – Coverage and Geometry. DSN Telecommunications Link Design Handbook (810-005), 2012.

[14] Jacobs, C. S. 107, Rev. A – Radio Source Catalog. DSN Telecommunications Link Design Handbook (810-005), 2011.

[15] McElrath, T. P., Watkins, M. M., Portock, B. M., Graat, E. J., Baird, D. T., Wawrzyniak, G. G., Guinn, J. R., Antresian, P. G., Attiyah, A. A., Baalke, R. C., and Taber, W. L. "Mars Exploration Rovers Orbit Determination Filter Strategy." Proceedings of the AIAA/AAS Astrodynamics Specialist Conference and Exhibit. Providence, RI, USA, 2004.

[16] Martin-Mur, T. J., Kruizinga, G. L., and Wong, M. C. "Mars Science Laboratory Interplanetary Navigation Analysis." 22nd International Symposium on Space Flight Dynamics. São José dos Campos, Brazil, 2011.